Identification of the Electron-Diffusion Region during Magnetic Reconnection in a Laboratory Plasma

Yang Ren,* Masaaki Yamada, Hantao Ji, Stefan P. Gerhardt, and Russell Kulsrud

Center for Magnetic Self-organization in Laboratory and Astrophysical Plasmas, Princeton Plasma Physics Laboratory, Princeton University, Princeton, New Jersey 08543, USA

(Received 21 January 2008; published 22 August 2008)

We report the first identification of the electron-diffusion region, where demagnetized electrons are accelerated to super-Alfvénic speed, in a reconnecting laboratory plasma. The width of the electron-diffusion region scales with the electron skin depth [$\sim(5.5–7.5)c/\omega_{pe}$] and the peak electron outflow velocity scales with the electron Alfvén velocity [$\sim(0.12–0.16)V_{eA}$], independent of ion mass.

DOI: 10.1103/PhysRevLett.101.085003 PACS numbers: 52.35.Vd, 52.72.+v

Magnetic reconnection is a process which converts magnetic energy to plasma kinetic and thermal energy [1]. Magnetic reconnection involves the breaking and reconnecting of magnetic field lines in a narrow ''diffusion region'' where the ideal ''frozen-in'' condition for the magnetic field is violated. The diffusion region, acting like a throttle, controls how fast plasma can flow through it and thus determines the magnetic energy release rate. Recent numerical results have shown that fast reconnection is facilitated by the Hall effect, the decoupling of ions from the magnetized electrons in the diffusion region [2]. The Hall effect leads to the formation of a two-scale diffusion region, in which a demagnetized electron-diffusion region is embedded in a much broader ion diffusion region.

In this Letter, we present the first identification of the electron-diffusion region, in which demagnetized electrons are accelerated to super-Alfvénic velocity, in the laboratory neutral sheet of the Magnetic Reconnection Experiment (MRX) [3]. The width of the electron-diffusion region scales with the electron skin depth [$\sim(5.5–7.5)c/\omega_{pe}$], and the peak electron outflow scales with the electron Alfvén velocity [$\sim(0.12–0.16)V_{eA}$], independent of ion mass. The identification of the electron-diffusion region is further supported by the direct measurement of the ion outflow, which is much slower and has a much wider width than the electron outflow.

According to recent 2D numerical simulations [2,4,5], the width of the electron-diffusion region is on the order of the electron skin depth, while the ion diffusion region is much wider, allowing the ions to flow out efficiently. A key signature of the Hall effect, a quadrupole out-of-plane magnetic field, has been observed in both space [6,7] and laboratory plasmas [8,9]. In addition, the electron-diffusion region has also been observed in space [10–12], where it was identified by examining the violation of the frozen-in condition for the electrons. Previously reported electron-diffusion regions in laboratory plasmas were either in electron magnetohydrodynamics plasmas [13] or in the presence of a strong guide field which magnetized the electrons [14]. To our knowledge, the direct demonstration of the decoupling of electrons from ions and the formation of a demagnetized electron-diffusion region in a laboratory neutral sheet has not been reported in the literature.

In MRX plasmas, the MHD criteria ($S \gg 1$, $\rho_i \ll L$, where S is the Lundquist number, ρ_i is the ion gyroradius, and L is the system scale length) are satisfied in the bulk of the plasma [3]. Figure 1 shows a cross section of the MRX vacuum vessel in the R-Z plane, and the positive toroidal direction defined points into the plane. The overall geometry of the device is axisymmetric, and thus global 2D geometry is ensured. Two toroidal plasmas with annular cross sections are formed inductively around the two flux cores [15]. By simultaneously reducing the toroidal current in both flux cores, the poloidal magnetic flux is pulled towards them, forming a current sheet and inducing magnetic reconnection. Five one-dimensional magnetic probe arrays, as shown in Fig. 1, are used to measure the profile of the out-of-plane magnetic field B_T in the R-Z plane with a spatial resolution up to 2.5 mm in the R direction and 3 cm in the Z direction. The in-plane current, $\mathbf{j}_{\text{in}}$, can be calculated from the out-of-plane magnetic field measurement using Ampere's law. We obtain the in-plane electron flow, $\mathbf{V}_{e,\text{in}}$, from $\mathbf{V}_{e,\text{in}} \approx -\mathbf{j}_{\text{in}}/(en_e)$, assuming that $|\mathbf{V}_i| \ll |\mathbf{V}_e|$. A Mach probe, which can be scanned in both the R and Z directions, is used to measure the ion outflow velocity, V_{iZ}. The plasma temperature and density are measured by two Langmuir probes (not shown). One of them is inserted radially and located at $Z = 0$. The other probe is inserted

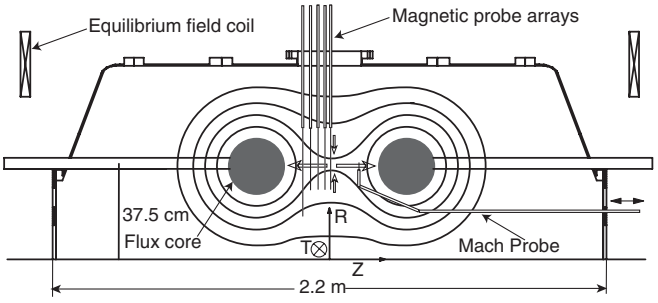

FIG. 1. Cross-sectional view of the MRX vacuum vessel, where the magnetic probe arrays and Mach probe are shown.

axially, like the Mach probe, and can be moved in the Z direction and can be scanned radially.

The electron-diffusion region is identified by evaluating the toroidal component of the generalized Ohm law across the reconnecting current sheet:

$$E_T + V_R B_Z = \eta_\perp j_T + \frac{j_R B_Z}{e n_e} - \frac{j_Z B_R}{e n_e}, \qquad (1)$$

where E_T is the reconnecting electric field, B_Z is the reconnecting magnetic field, B_R is the radial magnetic field, V_R is the ion inflow velocity, $\eta_\perp$ is the perpendicular Spitzer resistivity, j_T, j_Z, and j_R are the three components of the current density, and e, m_e, and n_e are the electron charge, mass, and density, respectively. Note that, in Eq. (1), we neglect the electron inertia term, the electron pressure term, and the terms from plasma turbulence—none of which were measured in the experiment. Three terms are evaluated from experimental data: E_T, $\eta_\perp j_T$, and $j_R B_Z/(e n_e)$. The reconnecting electric field is calculated from $E_T = \dot{\Psi}/2\pi R$, where Ψ is the poloidal flux function [16]. The reconnecting magnetic field B_Z is measured by the probe array at $Z = -3$ cm with a resolution up to 0.5 cm in the R direction. The j_T profile is calculated by fitting the measured reconnecting field to the Harris sheet profile [17]. Figure 2(a) plots the radial profiles of these terms. Since we do not have good B_R measurements close to the X line, we are not able to evaluate the radial profile of the $j_Z B_R/(e n_e)$ term. However, since this term peaks only at the current sheet center due to the peaked profile of j_Z, we need only to estimate the magnitude of this term. The value of B_R at $Z = -6$ cm is about 30 G, measured by a coarse magnetic probe array [8]; we use the linearly interpolated value of 15 G as the estimate of the value of B_R at $Z = -3$, noting that $B_R = 0$ at $Z = 0$. Thus we find that the magnitude of $j_Z B_R/(e n_e)$ is about 50 V/m in the current sheet center.

In Fig. 2(a), it is clear that far away from the current sheet center (at $R \approx 37.5$ cm) the electron frozen-in condition, $E_T + V_{eR} B_Z = E_T + V_R B_Z - j_R B_Z/(e n_e) = 0$, must be satisfied, and thus $V_R B_Z$ is evaluated from $V_R B_Z = -E_T + j_R B_Z/(e n_e)$. The resulting $V_R B_Z$ is positive, which shows that the ions are flowing towards the X line, but the ion frozen-in condition is broken, since $E_T + V_R B_Z \neq 0$. This violation of the ion frozen-in condition shows that this region is the ion diffusion region, although the boundaries of the ion diffusion region are beyond the measurement area. The two vertical dashed lines in Fig. 2(a) denote the positions where $E_T - j_R B_Z/(e n_e) \approx 0$, which demonstrates that the ions have been completely decoupled from the magnetic field lines since $V_R B_Z$ becomes much smaller than $-E_T$; i.e., $|V_R| \ll |E_T/B_Z|$, where $|E_T/B_Z|$ represents the velocity of the magnetic field lines. The shaded region between the vertical dashed lines is the electron-diffusion region, where $-(j_R B_Z - j_Z B_R)/(e n_e)$ becomes significantly less than $-E_T$ [note that, as discussed above, the magnitude of $j_Z B_R/(e n_e)$ is about 50 V/m, much smaller than $-E_T \approx 170$ V/m]. Since $|V_R| \ll |V_{eR}|$ and $|V_Z| \ll |V_{eZ}|$ (shown in Fig. 3), where V_Z is the ion outflow velocity, the electrons are decoupled from the magnetic field lines. It is obvious in Fig. 2(a) that the collisional resistive term, $-\eta_\perp j_T \approx 40$ V/m, is not large enough to balance $-E_T - j_Z B_R/(e n_e)$, which is about 120 V/m, in the electron-diffusion region. The electron inertia term, the electron pressure term, and the fluctuation terms, not shown in Eq. (1), can contribute to balance E_T, although the study of the exact roles of these terms is beyond the scope of this Letter.

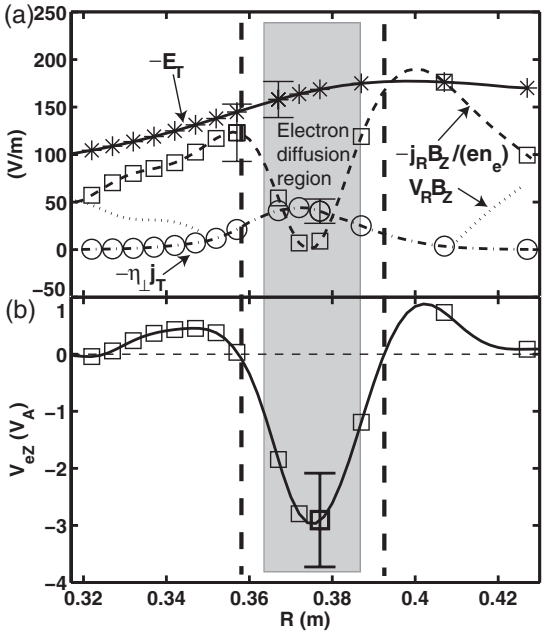

FIG. 2. (a) Radial profiles of four terms in the generalized Ohm law: the reconnecting electric field ($-E_T$) (solid line), the Hall term $[-j_R B_Z/(e n_e)]$ (dashed line), the collisional resistive term ($-\eta_\perp j_T$) (dash-dotted line), and $V_R B_Z$ (dotted line) measured in a helium plasma with a fill pressure of 8 mTorr. The corresponding symbols show the coil positions. The error bars result from the uncertainties in the magnetic field, density, and temperature measurements. All quantities are evaluated at $Z = -3$ cm. The shaded area denotes the electron-diffusion region, where $E_T + V_{eR} B_Z - V_{eZ} B_R \neq 0$. (b) The radial profile of the electron outflow velocity V_{eZ} at $Z = -3$ cm. The two vertical dashed lines denote the positions where $E_T - j_R B_Z/(e n_e) \approx 0$.

In Fig. 2(b), we plot the electron outflow velocity V_{eZ} as a function of R, where the two vertical lines and the electron-diffusion region are positioned the same as in Fig. 2(a). The two vertical lines coincide with the edges of the electron outflow channel, where the electrons flow toward the outflow region, i.e., $V_{eZ} < 0$. Thus we conclude that the width of the electron-diffusion region is consistent with the width of the electron outflow channel. We define the width of the electron outflow channel, δ_{BT}, as the half width where the electron outflow velocity decreases to 40% of its peak value. The defined δ_{BT} also represents the width of the electron-diffusion region, and this definition will be used in the rest of this Letter.

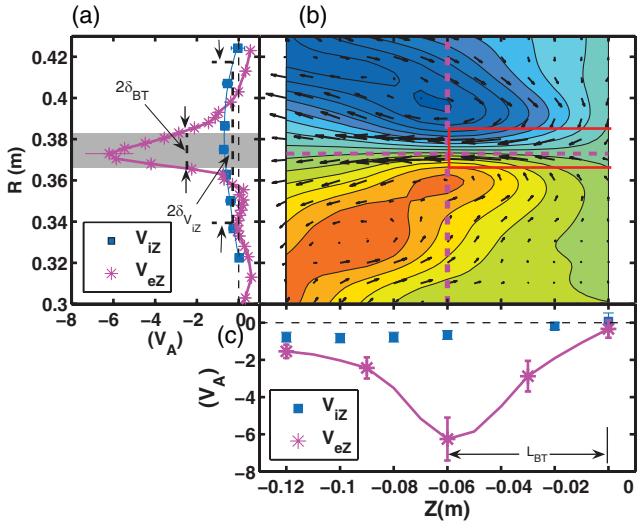

FIG. 3 (color). (a) The radial profiles of the electron outflow velocity, V_{eZ} (magenta asterisks), and ion outflow velocity, V_{iZ} (blue squares), measured in a helium plasma with a fill pressure of 8 mTorr. (b) The two-dimensional profile of B_T (color-coded contours) and $\mathbf{V}_e$ (black arrows). (c) V_{eZ} and V_{iZ} as a function of Z. V_{eZ} and V_{iZ} are normalized to V_A, the Alfvén velocity based on the shoulder reconnecting field and central density. The magenta dashed lines in (b) represent the cuts at $Z = -6$ cm and $R = 37.5$ cm, along which the profiles in (a) and (c) are taken. Note that V_{eZ} peaks at $Z = -6$ cm and $R = 37.5$ cm. The magenta and blue solid lines in (a) and (c) are the interpolations of V_{eZ} and V_{iZ}, respectively. In (a), δ_{BT} and $\delta_{V_{iZ}}$ are the widths of the electron-diffusion region and ion outflow channel, respectively ($\delta_{V_{iZ}}$ uses the same definition as δ_{BT}), and the shaded region shows the electron-diffusion region. In (c), L_{BT} denotes the electron acceleration length and is defined as the length of the electron-diffusion region. A red half-open box in (b), with a width of $2\delta_{BT}$ and length of L_{BT}, shows the electron-diffusion region.

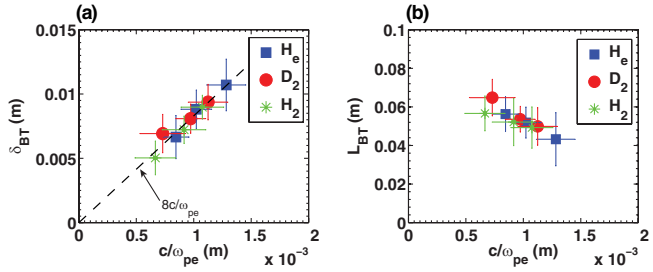

FIG. 4 (color online). (a) δ_{BT} as a function of c/ω_{pe}; (b) L_{BT} as a function of c/ω_{pe}. c/ω_{pe} is calculated using the central density in the electron-diffusion region. Discharges with three different ion species are shown: helium (solid squares), deuterium (solid circles), and hydrogen (asterisks). The dashed line ($\delta_{BT} = 8c/\omega_{pe}$) is the linear best fit to the data in (a). See text for the definitions of δ_{BT} and L_{BT}.

To support our identification of the electron-diffusion region, here we show the direct evidence for the decoupling of the ions and electrons. Figure 3(a) shows the radial profiles of V_{eZ} and V_{iZ}, where V_{eZ} is calculated from $V_{eZ} = -j_Z/(en_e) + V_{iZ}$, at the Z location where V_{eZ} peaks. Figure 3(b) plots the profile of B_T in the R-Z plane, showing half of the out-of-plane quadrupole field. Figure 3(c) shows the profiles of V_{eZ} and V_{iZ} in the Z direction at $R = 37.5$ cm where V_{eZ} peaks. In Fig. 3(a), it is obvious that V_{eZ} is much larger than V_{iZ} in the electron-diffusion region (the shaded region), showing that the approximation $\mathbf{V}_e \approx -\mathbf{j}/(en_e)$ is justified there. The width of the electron-diffusion region, δ_{BT}, and the width of the ion outflow channel, $\delta_{V_{iZ}}$, are about 0.7 and 4 cm, respectively. This large difference illustrates that the ions decouple from magnetic field lines (to form the ion outflow channel) on a much larger spatial scale than do the electrons, demonstrating the formation of two diffusion regions. As shown in Fig. 3(c), the length of the electron-diffusion region, L_{BT}, is defined as the distance over which the electrons are accelerated to their maximum speed. This definition is consistent with that used in numerical simulations [4,5]. A red half-open box, with a width of $2\delta_{BT}$ and a length of L_{BT}, shows the electron-diffusion region in Fig. 3(b). It is clear that the electron-diffusion region is the region where the electrons stop flowing towards the X line and are accelerated in the Z direction.

Having identified the electron-diffusion region, the scalings of its width and length can be studied by varying the plasma density and ion species. Figure 4(a) plots δ_{BT} as a function of the electron skin depth (c/ω_{pe}). The error bars come mainly from shot-to-shot variation. The data points with different ion species come together on one line, demonstrating that δ_{BT} scales only with the plasma density and has no dependence on ion mass. A linear relation between δ_{BT} and the electron skin depth can be obtained from Fig. 4(a): $\delta_{BT} \approx 8c/\omega_{pe}$. With corrections due to the current blockage by the magnetic probe, the thickness changes to $\delta_{BT} \approx (5.5\text{–}7.5)c/\omega_{pe}$ [18]. This scaling of the electron-diffusion region is consistent with theory and numerical results [4,5,18], although a different coefficient was found there: $\delta_{BT} \approx (1\text{–}2)c/\omega_{pe}$. In Fig. 4(b), L_{BT} is plotted as a function of c/ω_{pe}. It is clear that the data points with different ion species again come together, which shows that L_{BT} has no ion mass dependence and is only a function of the plasma density. For deuterium and helium plasmas, L_{BT} tends to decrease as the plasma density is lowered. The same relationship is also present for hydrogen plasmas but is less clear due to the large error bars. This relationship agrees with previous observations in MRX [19], where the current sheet length is found to decrease when the fill pressure (and thus the plasma density) is lowered. The length of the electron-diffusion region has been addressed in numerical simulations [4,5]. In Ref. [4], L_{BT} is found to scale with the electron skin depth, $\sim 5c/\omega_{pe}$. Here we have verified that L_{BT} does not depend on ion mass, which agrees with the simulation. However, we also find that L_{BT} [$\sim(40\text{–}80)c/\omega_{pe}$], which is not only much larger than the $5c/\omega_{pe}$ found in the simulation, but

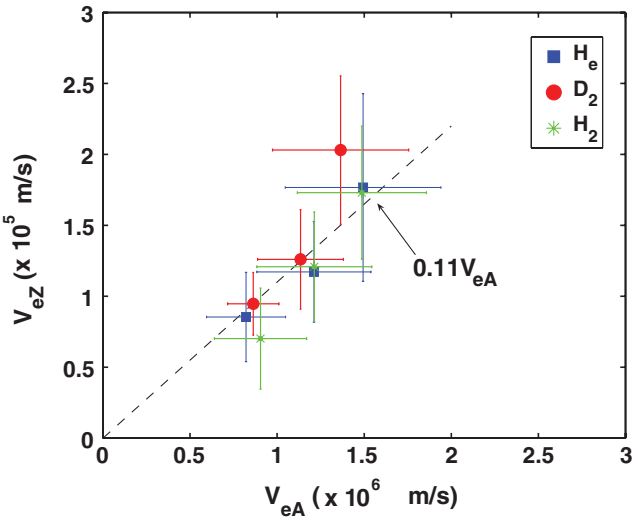

FIG. 5 (color online). The peak electron outflow velocity, V_{eZ}, as a function of V_{eA}. Discharges with three different ion species are shown: helium (solid squares), deuterium (solid circles), and hydrogen (asterisks). The dashed line ($V_{eZ} = 0.11V_{eA}$) is the linear best fit to the data.

does not scale with c/ω_{pe} either. More recent numerical simulations [5,20] shows that the electron-diffusion region can extend to tens of c/ω_{pi} in length when a large simulation domain (several hundred c/ω_{pi}), with either open or periodic boundary conditions, is used. Note that L_{BT} is about $(1–2)c/\omega_{pi}$ in the experiment, which is much less than tens of c/ω_{pi}. However, this difference could be due to the size of the experiment, i.e., the distance (40 cm) between two flux cores shown in Fig. 1 which corresponds to about $14c/\omega_{pi}$ in a high density hydrogen discharge. Note that even fewer c/ω_{pi} can fit in the experiment as the plasma density is lowered. The length of the electron-diffusion region will be addressed in future experiments where the distance between the flux cores will be varied.

Since the outflow velocity affects the reconnection rate, we plot the maximum electron outflow velocity, V_{eZ}, against the electron Alfvén velocity, V_{eA}, in Fig. 5, from plasmas with three different ion species (the electron Alfvén velocity is calculated with the reconnecting magnetic field evaluated at the edge of the electron-diffusion region and the central density). Note that the data shows no ion mass dependence within error bars, since the points come together on a single line despite the variation in the ion species. The measured V_{eZ} scales with the electron Alfvén velocity, namely, $V_{eZ} \approx 0.11V_{eA}$, indicted by the linear best fit shown in the figure. We note that with the same probe effect corrected, the above scaling changes to $V_{eZ} \approx (0.12–0.16)V_{eA}$. This result is different from numerical results [4,5] where $V_{eZ} \approx V_{eA}$. However, we point out that although the measured V_{eZ} is much slower than V_{eA} as predicted by the numerical results, the width of the electron-diffusion region is also wider in the experiment than the simulations. Thus the total electron flux from the electron-diffusion region is $n_e V_{eZ}\delta_{BT} \approx 0.9 n_e V_{eA} c/\omega_{pe}$, consistent with theory and numerical results [4,21]. We note that the above calculation of the total electron flux is not affected by the probe effect since the effect increases δ_{BT} and reduces V_{eZ} simultaneously.

In summary, we have identified the demagnetized electron-diffusion region during Hall-mediated fast magnetic reconnection for the first time in a laboratory plasma. The width of the electron-diffusion region is found to be consistent with that of the electron outflow channel. Both the width and the length of the electron-diffusion region have no ion mass dependence, and the width of the electron-diffusion region scales with the electron skin depth as $(5.5–7.5)c/\omega_{pe}$. This width is much larger than that in Hall-MHD simulation [4] and even that in 2D full kinetic simulations [5], which implies the 2D simulations may be missing important physics. The maximum electron outflow velocity in the experiment scales with the electron Alfvén velocity as $(0.12–0.16)V_{eA}$. However, since the width of the electron-diffusion region is wider in the experiment than numerical results [4,5], the total electron flux from the electron-diffusion region remains consistent with theory and simulations.

The authors thank D. Cylinder and R. Cutler for their excellent technical support. The authors also thank H. Torreblanca for his assistance on the Mach probe measurement. This work was jointly supported by DOE, NASA, and NSF.

*Present address: University of Wisconsin-Madison, USA.

[1] P. A. Sweet, *The Neutral Point Theory of Solar Flares* (Cambridge University Press, Cambridge, England, 1958).
[2] J. Birn *et al.*, J. Geophys. Res. **106**, 3715 (2001).
[3] M. Yamada *et al.*, Phys. Plasmas **4**, 1936 (1997).
[4] M. A. Shay *et al.*, J. Geophys. Res. **106**, 3759 (2001).
[5] W. Daughton *et al.*, Phys. Plasmas **13**, 072101 (2006).
[6] X. H. Deng and H. Matsumoto, Nature (London) **410**, 557 (2001).
[7] M. Oieroset *et al.*, Nature (London) **412**, 414 (2001).
[8] Y. Ren *et al.*, Phys. Rev. Lett. **95**, 055003 (2005).
[9] M. R. Brown *et al.*, Phys. Plasmas **13**, 056503 (2006).
[10] J. D. Scudder *et al.*, J. Geophys. Res. **107**, 1294 (2002).
[11] F. S. Mozer *et al.*, Phys. Rev. Lett. **91**, 245002 (2003).
[12] T. D. Phan *et al.*, Phys. Rev. Lett. **99**, 255002 (2007).
[13] R. L. Stenzel and W. Gekelman, Phys. Rev. Lett. **42**, 1055 (1979).
[14] J. Egedal *et al.*, Phys. Rev. Lett. **90**, 135003 (2003).
[15] M. Yamada *et al.*, Phys. Rev. Lett. **46**, 188 (1981).
[16] H. Ji *et al.*, Phys. Rev. Lett. **80**, 3256 (1998).
[17] M. Yamada *et al.*, Phys. Plasmas **7**, 1781 (2000).
[18] H. Ji *et al.*, Geophys. Res. Lett. **35**, L13106 (2008).
[19] A. Kuritsyn *et al.*, Geophys. Res. Lett. **34**, L16106 (2007).
[20] M. A. Shay *et al.*, Phys. Rev. Lett. **99**, 155002 (2007).
[21] M. E. Mandt *et al.*, Geophys. Res. Lett. **21**, 73 (1994).